Article

Synthesis of all-inorganic halide perovskite nanocrystals for photocatalysis applications

Xiaoqian Wang [1], Wanli Liu [1], Jiazhen He[1], Yuqing Li[1] and Yong Liu [1]*

[1]International School of Materials Science and Engineering (ISMSE), State Key Laboratory of Advanced Technology for Materials Synthesis and Processing, Wuhan University of Technology, Wuhan 430070, China 303568@whut.edu.cn.

* Correspondence: liuyong3873@whut.edu.cn

Abstract: Compared with conventional semiconductors, halide perovskite nanocrystals (NCs) have a unique crystal structure and outstanding optoelectronic properties, which offer a wide potential for applications in optoelectronic devices such as solar cells, photodetectors, light emitting diodes, lasers and displays. Rational technological design is providing vital support for the development of perovskite optoelectronics. Herein, high-quality and monodisperse all-inorganic halide perovskite nanocrystals with consistent morphology, concentrated size distribution and cubic crystal phase were synthesized employing a modified one-pot hot injection method to independently modulate the stoichiometric ratios of three precursors involving cesium salt, lead source and halide. Mixing two kinds of perovskite NCs with different halogens, in combination with an anion exchange reaction, enables a transition from violet emission to green and finally to red emission over the entire visible region. Our work will be applied to enhance optoelectronic properties and stability of all-inorganic perovskite NCs for serving as light-emitting components in optoelectronic devices, as well as expanding the application areas of perovskite semiconductors for photocatalytic hydrogen generation, CO_2 reduction and dye degradation.

Keywords: synthesis; $CsPbX_3$; perovskite nanocrystals

1. Introduction

Over the past years, halide perovskite materials have developed dramatically as a novel, solution-processable ionic semiconductor with a direct band gap. Comparing to conventional semiconductors, it possesses a unique structure which can be expressed as ABX_3 (X = Cl^-, Br^-, I^-) [1]. Where the A-site is a monovalent cation with a relatively small radius, which can be Cs+, ($CH_3NH_3^+$) MA^+, ($[HC(NH_2)_2]^+$) FA^+, and B-site is occupied by divalent metal cations such as Pb^{2+}, Sn^{2+}, while X-site is a halogen anion [2-6]. In the cubic halide perovskite crystal structure, six X^- and B^{2+} are connected to create a covalent top-linked $[BX_6]^{4-}$ coordinated octahedron, B-site ion located at the octahedral center, with the A-site cation populating octahedral vacancies, which enables charge balance [7].

The structure of halide perovskite allows it to display superior optoelectronic properties, including high absorption coefficient, extremely large photoluminescence quantum yield (PLQY), pure color emission and variable band gap [8-10]. Among them, PLQY of the red-emitting $CsPbI_3$ is already close to 100% [11]. Owing to its soft ionic nature and strongly ionic interactions with surface ligands, it makes it facile for anion exchange to occur between perovskite nanocrystals (NCs) of different halogens, which can be utilized for flexible band gap width modulation (1.78-3.1 eV), and to control fluorescence wavelength covering the entire visible spectral range [9, 12]. In addition, the enhanced quantum confinement effect of halide perovskite can also be harnessed to tailor optical absorption and luminescence performance[13]. Electrically, halide perovskite characterized by long

 doi:10.20944/preprints202306.0354.v1

charge diffusion lengths and high carrier mobility [14, 15]. By means of time-resolved terahertz spectroscopy, $CsPbBr_3$ NCs were discovered to boast extremely high free carrier dynamics, with carrier mobilities of up to 4500 $cm^2\ V^{-1}\ s^{-1}$ and diffusion lengths greater than 9.2 μm, which render their intrinsic transport properties ideal[14]. Thus, halide perovskite holds great value for optoelectronic applications and offers a wide scope of prospects in high-efficiency solar cells [16-18], sensitive photodetectors[19-21], low-threshold lasers [22-24],light-emitting diodes (LEDs) [25-27], scintillators [28-30], and bioimaging systems [31-33]. Among the multitude of applications, metal halide perovskite is particularly impressive in the field of solar cells. In the short span of a decade or so, photoelectric conversion efficiency (PCE) has increased from an initial 3.8% to 25.5%, comparable to mature silicon-based solar cells [16]. Inspired by it, halide perovskites provide the ability to separate electron-hole pairs and can be employed as a novel photocatalyst for hydrogen precipitation [34-36], CO_2 reduction [37-40], and dye degradation [41, 42].

The superior stability of all-inorganic $CsPbX_3$ perovskite materials compared to organic-inorganic hybrid halide perovskites is attributed to the sensitivity of organic molecules (such as MA^+) to light, heat, moisture, and irradiation, which decomposes or damages the structure, limiting its application in storage, fabrication, and equipment manipulation process [43-45]. The choice of synthesis technique will likewise have an impact on stability of a material. Up to now, methods for the direct synthesis of all-inorganic perovskite comprise both solution-processed and vapor phase methods. The vapor phase method deposits perovskite single crystals or arrays on a substrate via a process of high temperature reactions [46, 47], while the solution-based process aims to regulate the size and dimension of the halide perovskites by controlling technical parameters such as precursors, the amount of surface ligands, chemical reaction temperature and duration [48, 49]. Nanoscale perovskite materials are a prerequisite for high performance optoelectronic applications. There are numerous approaches to the synthesis of promising NCs, with ligand-assisted reprecipitation, solvothermal and hot injection methods are effective and proven strategies. The synthesis protocol of solvothermal method is relatively simple and controllable [50]. The precursors are usually mixed with a nonaqueous solvent and kept in a closed container such as a stainless steel autoclave, where cesium acetate (cesium oleate) and halide lead will react to produce $CsPbX_3$ NCs under a certain temperature and self-generated pressure of the solution [51]. Ligand-assisted reprecipitation approach is based on the recrystallization of ligand halide salts, in which the metal halide salt is dissolved in a polar solvent and subsequently dropped into a nonpolar medium in the presence of the ligand to trigger the recrystallization of NCs [52]. In general, hot injection method involves the synthesis of NCs by injecting cesium oleate into a lead halide solution under an inert atmosphere [8]. The aforementioned approaches are restricted in that the PbX_2 applied as lead and halogen sources, which make it impossible to directly adjust the stoichiometric ratios of the two elements individually. The result is that the NCs are susceptible to damage through irradiation and are less stable under transmission electron microscopy. Hence, improved hot injection methods are essential to govern structural stability and optoelectronic properties of all-inorganic halide perovskite NCs.

Here, we employ a modified one-pot hot injection method to synthesize monodisperse and uniformly sized $CsPbX_3$ perovskite nanocrystals (NCs) by independently manipulating the stoichiometric ratios of Cs^+, Pb^{2+} and X^-. Their cubic crystal structure and high phase purity were demonstrated by XRD analysis. The findings of Fourier transform infrared spectroscopy (FTIR) revealed the validated protonation of oleylamine on the surface of $CsPbBr_3$ nanocrystals. In addition, the presence of a single narrow emission peak in the fluorescence spectra of perovskite nanocrystals is driven by different halogen compositions, giving rise to varying band gaps and therefore differential fluorescence absorption and emission peak positions. Accompanied by the red shift of the fluorescence wavelength (narrowing of the band gap), the PL lifetime of the $CsPbCl_3$, $CsPbBr_3$ and $CsPbI_3$ NCs grow larger and their decay rate slows down. The mixture of NCs with different halogens is susceptible to carry out anion exchange reactions, allowing the absorption

Preprints (www.preprints.org) | NOT PEER-REVIEWED | Posted: 5 June 2023 doi:10.20944/preprints202306.0354.v1

peaks of the nanocrystals to be tuned from 400nm to 700nm. And their color of the nanocrystals to be gradually tuned from violet to red under 365nm UV lamp excitation, covering the entire visible range. The well-defined morphology and excellent optoelectronic properties will boost the application of all-inorganic halide perovskite NCs in optoelectronic devices and photocatalysis.

2. Results and discussion

It is crucial that the high-quality synthesis of all-inorganic halide perovskite nanocrystals (NCs) is worthwhile for effective implementation of superior performance of optoelectronic devices. In particular, the selecting of suitable precursors and reaction conditions are vital factors influencing the quality of the NCs. For the common hot injection method, cesium oleate is injected into a solution of lead halide (PbX_2) for reaction to transform into perovskite [8]. Cesium oleate is prone to solidify at room temperature and requires to be preheated before the process of injecting. As opposed to this, we will take the option of incorporating benzoyl halides, injecting them into metal cation (Cs^+, Pb^{2+}) salt solutions, which not only will provide a halogen-rich environment, but also facilitate the effective protonation of the oleylamine (OAm). In our typical synthetic process, Cs_2CO_3 and $Pb(CH_3COO)_2{\cdot}3H_2O$ were applied as cesium source and lead source respectively, OA and OAm were chosen as surface ligands as well as ODE as the solvent. The reaction system was kept under vacuum by removing excess air and water by evacuating at 130 °C for 1h. Subsequently, $CsPbI_3$, $CsPbBr_3$ and $CsPbCl_3$ NCs were immediately synthesized by metathesis reactions via rapidly injecting benzoyl halides under N_2 at 165 °C, 170 °C and 200 °C (**Scheme 1** and more details in the **Materials and Methods** section). In contrast to the conventional hot injection method, it was possible to produce well distributed perovskite NCs as a result of the independent control of the stoichiometric ratios of origin of Cs^+, Pb^{2+} and X^- instead of employing PbX_2 as both the lead and halogen sources. In addition, a series of subsequent centrifugation procedures facilitated the final monodisperse cubic NCs hexane dispersed solution, which contributed to substantially improved performance of optoelectronic devices.

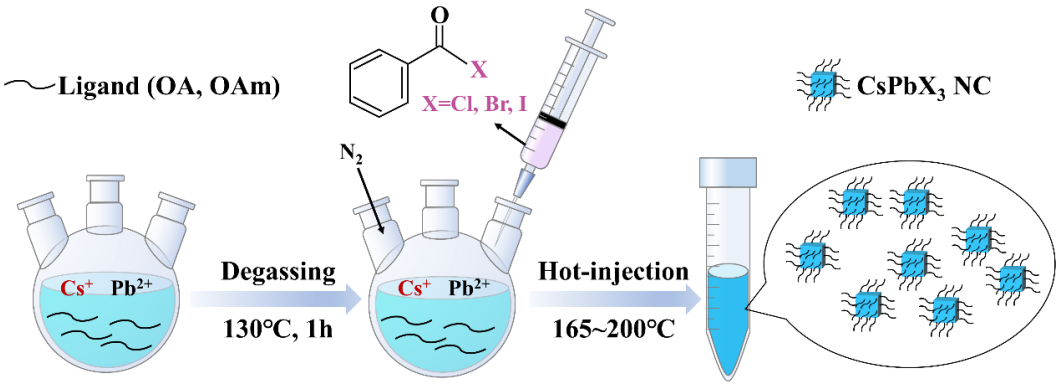

Scheme 1. Schematic diagram of the synthesis procedure of all-inorganic $CsPbX_3$ (X = Cl, Br, I) perovskite NCs.

As shown in **Figure 1**, TEM images of $CsPbCl_3$, $CsPbBr_3$ and $CsPbI_3$ nanocrystals (NCs) display that they present uniform and monodisperse cubic structures. Under electron microscopic irradiation, three NCs did not instantly decompose into white cubes and irregular black spots located in the corners, keeping their shape and structure more integrated. Naturally, if irradiated on a continuous manner, the high-energy electron beam will damage the structure of perovskite NCs and the decomposition products might be PbX_2, CsX, or CsPb [53]. It was reported that the resistance of halide perovskite NCs to exposure to irradiation could be enhanced in the manner of supplementing the amount of

Preprints (www.preprints.org) | NOT PEER-REVIEWED | Posted: 5 June 2023 doi:10.20944/preprints202306.0354.v1

halogen ions [54]. Exactly, our synthesis procedure is equipped with the ability to independently manipulate the stoichiometric ratio of elements composed of halide perovskite, which can effectively improve the irradiation stability of perovskite NCs. In addition to the halogen content, temperature and electron beam dose also have an influence on the morphology of all-inorganic halide perovskite. Incident electrons will trigger the desorption of halogen ions from the $CsPbBr_3$ surface, which takes place with the evolution of the electron dose, moreover low temperatures can be introduced to inhibit ion migration [53]. Therefore, in order to avoid (reduce) irradiation damage, it is possible to take some measures such as changing the electronic irradiation dose and decreasing the working temperature of transmission electron microscope (or directly employing cryo-electron microscopy) when capturing TEM images [55]. Additionally, 300 NCs were selected to measure their size and analysis of the results indicated a concentrated distribution of sizes, as well as their average sizes of $CsPbCl_3$: 9.97 ± 0.20 nm, $CsPbBr_3$: 9.61 ± 0.13 nm and $CsPbI_3$: 15.12 ± 0.14 nm, respectively.

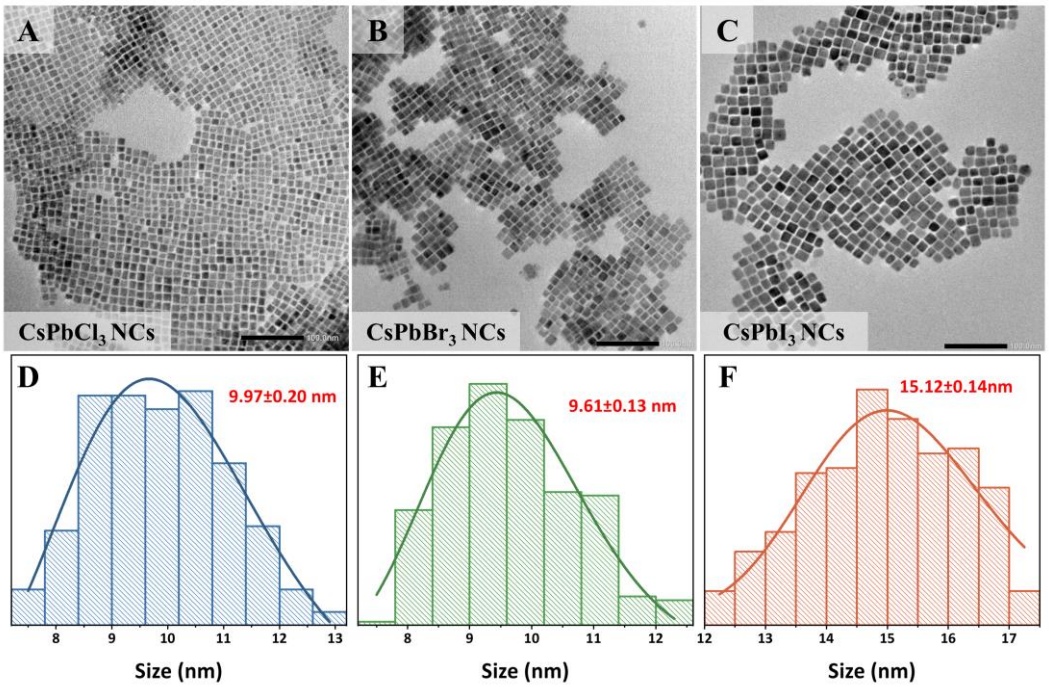

Figure 1. (A-C) TEM images of $CsPbCl_3$, $CsPbBr_3$ and $CsPbI_3$ NCs, respectively (Scale bar: 100 nm) and (D-F) their size distribution diagrams.

X-ray diffraction (XRD) and Fourier transform infrared spectroscopy (FTIR) are available to characterize the structure and surface functional groups of materials. In **Figure 2A-C**, XRD patterns obtained for the three different halogens of perovskite NCs were analyzed and we discovered to be well matched to cubic perovskite crystals. The corresponding ICSD numbers for $CsPbCl_3$, $CsPbBr_3$ and $CsPbI_3$ NCs are 23108, 29073 and 181288, respectively, corresponds to space group $pm\bar{3}m$ (No. 221). The diffraction peaks in the vicinity of $2\theta \approx 15°$, 20° and 30° for all three types of perovskite nanocrystals corresponding to the (100), (110) and (200) crystallographic planes. However, there is a notable divergence in the diffraction peak positions associated with the (210), (211) and (220) crystal planes of NCs, with $CsPbCl_3$ at 35.8°, 39.3° and 45.7°, respectively; whereas $CsPbBr_3$ at 34.1°, 37.4° and 43.5°, respectively; and $CsPbI_3$ near 31.9°, 35° and 40.7°, respectively. The diffraction angles corresponding to the same diffraction crystal plane of the perovskite NCs will change depending on the halogen component. From $CsPbCl_3$ to $CsPbBr_3$ to $CsPbI_3$, the diffraction peaks appear to be shifted in the direction of a small angle. Based on Bragg equation $2d\sin\theta = n\lambda$ (d is the spacing between crystal planes, θ is the diffraction

Preprints (www.preprints.org) | NOT PEER-REVIEWED | Posted: 5 June 2023 doi:10.20944/preprints202306.0354.v1

half angle, and n is the diffraction order), it is known that their corresponding crystal plane spacing gets larger. In the FTIR spectrum of $CsPbBr_3$ NCs (**Figure 2D**), we observed peak positions of 2925, 1379 and 2854 cm^{-1} indicating asymmetric and symmetric stretching vibrations of the C-H single bond, respectively, while absorption peaks of 1466 and 721 cm^{-1} representing in-plane bending vibrations of the C-H single bond in the $-CH_2-$ group. Whereas the peaks at 993, 909 and 801 cm^{-1} represent the bending vibration of =C-H, which originate from OA and OAm. The peak at 1536 cm^{-1} can be attributed to the C=O bond from the -COO- group of OA. Especially, the absorption peak located at a wave number of 1642 cm^{-1} denotes a deformational vibration of the N-H bond corresponding to $-NH_3^+$, which arises from the OAm. The appearance of differential absorption peak positions in the FTIR spectra is indicative of a variation in the vibrational mode of the functional groups, thereby demonstrating the effective protonation of the oleylamine on the surface of the $CsPbBr_3$ NCs.

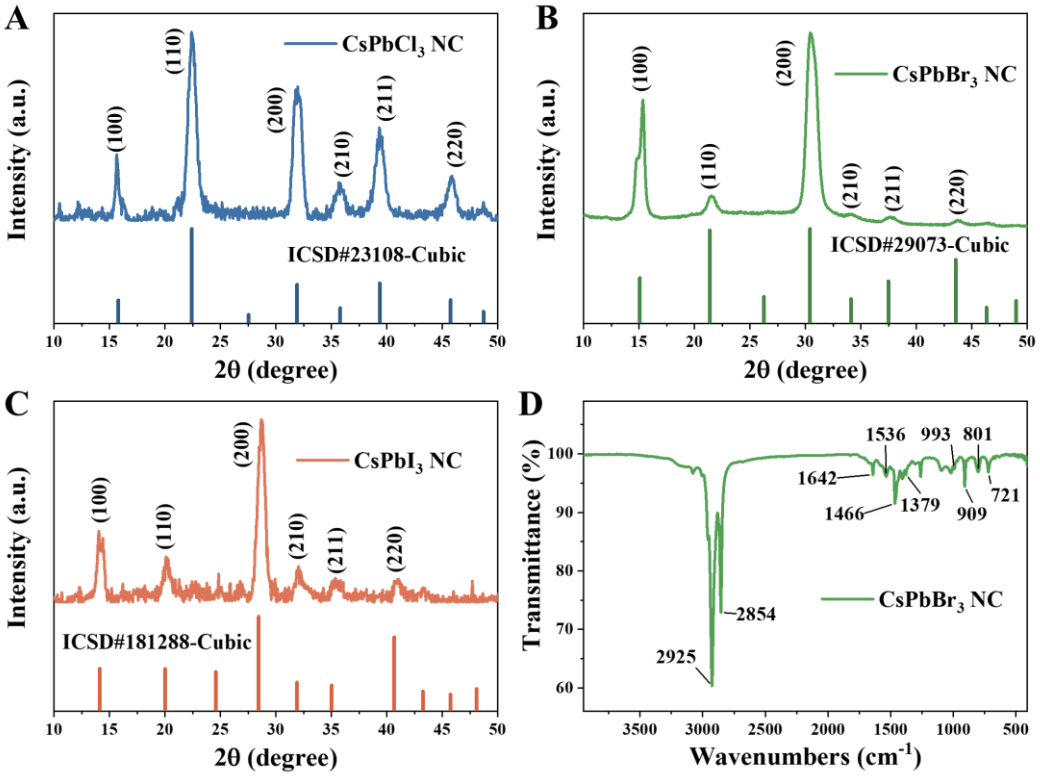

Figure 2. (A-C) XRD patterns of $CsPbX_3$ (X = Cl, Br, I) NCs. (B) FTIR spectra of $CsPbBr_3$ NCs.

Later, we measured the fundamental optical properties of three NCs, including UV-vis absorption spectra, PL and TRPL spectra (**Figure 3**). The band edge peak positions of the $CsPbCl_3$, $CsPbBr_3$ and $CsPbI_3$ NCs are at 402 nm, 506 nm and 675 nm, respectively. The absorption spectra exhibit two or three exciton leap peaks as a result of the quantum confinement effect, indicating the smaller size and better homogeneity of the all-inorganic perovskite NCs prepared by our scheme. The fluorescence emission peaks in the PL spectra are 411 nm, 521 nm and 694 nm, respectively, and the corresponding Stokes shifts due to quantum confinement effects are calculated to be 9 nm, 15 nm and 19 nm, respectively. The average fluorescence lifetimes of $CsPbX_3$ (X = Cl, Br, I) NCs were 11.29 ns, 12.92 ns and 49.26 ns respectively through a third order exponential fitting from TRPL curves (**Figure 3D**). The different ionic radii of the three halogens, Cl^-, Br^- and I^-, in turn become larger, leading to a variation in the volume of their vacancies in the perovskite crystal structure, which allows the optical band gap of the perovskite NCs to shift from $CsPbCl_3$, $CsPbBr_3$ to $CsPbI_3$ to become smaller in turn, corresponding to a gradual red shift in fluorescence

Preprints (www.preprints.org) | NOT PEER-REVIEWED | Posted: 5 June 2023 doi:10.20944/preprints202306.0354.v1

wavelength. Furthermore, only a narrow emission peak appears in the fluorescence spectrum with a high photoluminescence quantum yield (PLQY). All-inorganic halide perovskite NCs possess huge potential to be applied in semiconductor light-emitting devices such as light-emitting diodes and displays on account of their excellent optical properties.

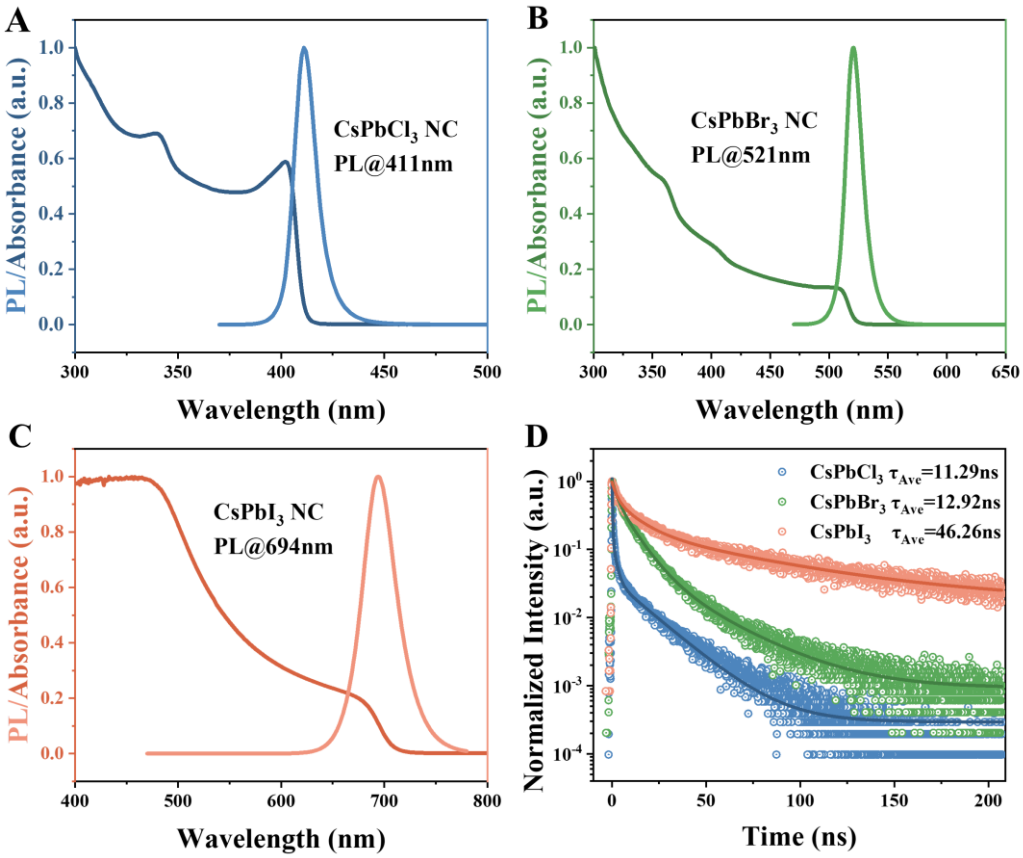

Figure 3. (A-C) UV-vis absorption and photoluminescence (PL) spectra of $CsPbCl_3$, $CsPbBr_3$ and $CsPbI_3$ NCs, respectively. (D) Time-resolved photoluminescence (TRPL) spectra of $CsPbCl_3$, $CsPbBr_3$ and $CsPbI_3$ NCs.

Given the ionic nature of perovskite and variability of surface ligands, anion exchange reactions readily occur between perovskite materials of diverse halogens. The common method adopted by researchers is to add metal halide salts of different halogens such as CuX_2 [56], KX [9], AlX_3 [57], ZnX_2 [54] to perovskite NCs, then stir the mixture for a period of time and eventually centrifugal separation to obtain perovskite with different halogen components. Instead, we mixed two types of perovskite nanocrystals with different halogens, and achieved different luminescence by ion exchange. The UV-vis spectra of the solutions of perovskite NCs with different halogen contents exhibited different absorption peak positions (**Figure 4A**), which were composed of $CsPbCl_3$, $CsPbBr_3$ with $CsPbCl_3$ volume ratio of 1:3, 3:1, $CsPbBr_3$, $CsPbBr_3$ with $CsPbI_3$ volume ratio of 3:1, 1:3, $CsPbI_3$ nanocrystal solutions, corresponding to the positions of the absorption peaks were 402 nm, 420 nm, 484 nm, 506 nm, 520 nm, 585 nm and 676 nm, respectively. Some samples were observed to feature two sharp exciton absorption peaks, while others appeared to be relatively smooth, which was attributed to the varying extent of quantum confinement effects caused by differences in size, concentration and homogeneity of the NCs. Perovskite nanocrystal solutions mixed in varying volume ratios behaved differently when stimulated with 365nm UV lamps. As illustrated in **Figure 4B**, the $CsPbCl_3$ NCs are purple and gradually change to blue and then green as Br^- increases when mixed with $CsPbBr_3$; the $CsPbBr_3$ NCs are green and gradually change to yellow-orange and finally red $CsPbI_3$

Preprints (www.preprints.org) | NOT PEER-REVIEWED | Posted: 5 June 2023 doi:10.20944/preprints202306.0354.v1

as I^- increases when mixed with $CsPbI_3$. We were also curious about the mixing of $CsPbCl_3$ with $CsPbI_3$ NCs, however, the reality is that the mixing of the two results in fluorescence extinction rather than fluorescence emission. According to the investigation, the plausible explanation is that the Cl^- and I^- radii are so distinct from each other that the mixing may enter each other's crystal structures in such a way as to cause damage. There is no very effective means of making $CsPbCl_3$ coexist with $CsPbI_3$ and maintaining two different fluorescence emissions at the same time.

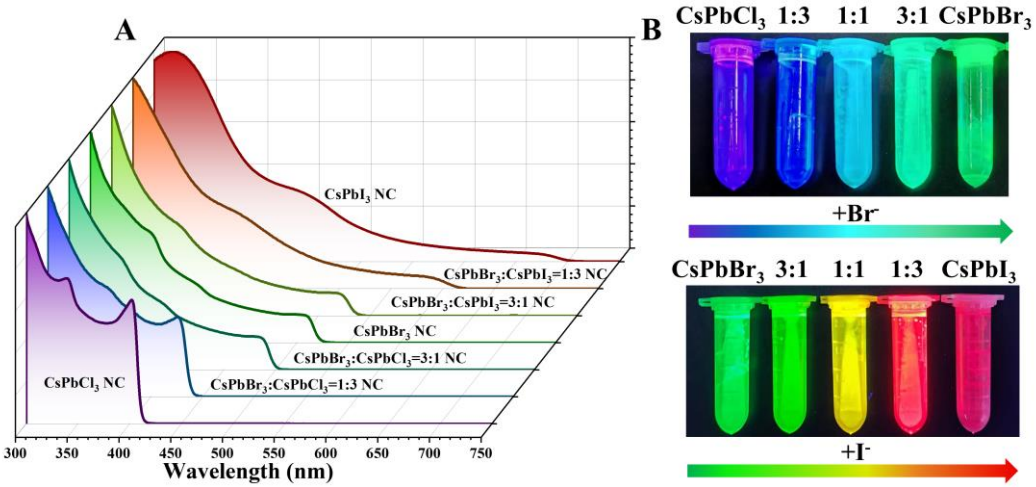

Figure 4. (A) UV-vis absorption spectra of perovskite NCs solutions with different volume ratios of $CsPbBr_3$ and $CsPbCl_3$, $CsPbBr_3$ and $CsPbI_3$. (B) Image of mixed solutions of $CsPbBr_3$ and $CsPbCl_3$ NCs with different volume ratios, and mixture of $CsPbBr_3$ and $CsPbI_3$ NCs with different volume ratios under 365 nm ultraviolet lamp excitation.

High-quality, pure cubic-phase all-inorganic perovskite $CsPbX_3$ (X = Cl, Br, I) NCs can be readily synthesized by an improved hot injection method. Analogous to conventional semiconductor NCs, halide perovskite NCs also exhibit nice homogeneity and monodispersity, well-defined cubic shapes, and high defect tolerance, which might be capable of self-assembling as building blocks into ordered superstructures, such as superlattices. The degree of ordering of perovskite superstructure will affect their optoelectronic properties and thereby alter the performance of functional electronic devices. When halogen ions are located at the octahedral vertices of the crystal structure of the perovskite NCs undergo changes, their UV-vis absorption positions and fluorescence emission peaks differentiate each other. As two NCs of different halogens are blended, the anion-exchange reaction gives rise to absorption and emission positions distinguishing them from $CsPbCl_3$, $CsPbBr_3$, and $CsPbI_3$ NCs. The variation in fluorescence emission colors is beneficial for the construction of white light emitting diodes (LEDs) with blue, green and red as ternary colors, which further enables their application in electronic displays. While due to their characteristic narrow, pure-colored fluorescence emission peaks, perovskite NCs can be exploited to make attempts to improve the performance of narrow linewidth lasers. Nevertheless, no devices were built to investigate the optoelectronic effect and photocatalytic properties, and we will complete subsequent studies.

3. Materials and Methods

3.1. Chemicals

Cesium carbonate (Cs_2CO_3, Aladdin, 99.9%), lead acetate trihydrate ($Pb(CH_3COO)_2{\cdot}3H_2O$, Aladdin, 99.99%), sodium iodide (NaI, Macklin, 99.99%), oleic acid (OA, Aladdin, AR), oleylamine (OAm, Aladdin, 80-90%), 1-octadecene (ODE, Aladdin,

Preprints (www.preprints.org) | NOT PEER-REVIEWED | Posted: 5 June 2023 doi:10.20944/preprints202306.0354.v1

>90%(GC)), benzoyl bromide (C_6H_5COBr, Aladdin, 97%), benzoyl chloride (C_6H_5COCl, Aladdin, 99%), n-hexane (Aladdin, >99%).

3.2. Synthesis Scheme of all-inorganic perovskite nanocrystals

3.2.1. Preparation of Benzoyl Iodine

The benzoyl iodine was synthesized following the method reported by Muhammad Imran. In a typical synthesis, sodium iodide (3 g, 0.2 mmol) and benzoyl chloride (1.4 ml) were mixed in a 20 ml vial. The mixture was stirred vigorously at 75 ℃ on a hot plate for 5 h. With heating and stirring, the mixture changed from white to orange red color, manifesting the successful synthesis of benzoyl iodine. Then, the mixture cooled to room temperature gradually and 5 ml of anhydrous ODE was added into the vial. The solution was filtered by a polytetrafluorethylene membrane with a 0.45 μm pore size to get clear benzoyl iodine stored in vacuum to further use.

3.2.2. Synthesis of $CsPbX_3$ (X = Cl, Br, I) Nanocrystals (NCs)

$CsPbX_3$ (X = Cl, Br, I) nanocrystals (NCs) were synthesized via the previously published procedures [58], with modifications. In a 50ml three-necked round-bottom flask, 0.016 g Cs_2CO_3, 0.076 g $Pb(CH_3COO)_2{\cdot}3H_2O$, 0.3 ml OA, 1 mL OAm, and ODE (5 ml for $CsPbCl_3$ and $CsPbBr_3$ NCs, 8 ml for $CsPbI_3$ NCs)were loaded and dried under vacuum at 130 ℃ for 1 h. When the reaction mixture had solubilized completely, the flask was heated up to 165~200 ℃ (The specific reaction temperatures are 200 ℃ for $CsPbCl_3$ NCs, 170 ℃ for $CsPbBr_3$ NCs and 165 ℃ for $CsPbI_3$ NCs, respectively) under a N_2 flow. Subsequently, benzoyl halides (1.8 mmol benzoyl chloride, 0.6 mmol benzoyl bromide and benzoyl iodine) were swiftly injected. The reaction mixture was cooled immediately with an ice bath to room temperature for $CsPbBr_3$ and $CsPbI_3$ NCs, while $CsPbCl_3$ NCs was cooled after 20 s to obtain crude solutions.

3.2.3. Isolaiton of $CsPbX_3$ (X = Cl, Br, I) Nanocrystals (NCs)

5 ml of n-hexane was added to the $CsPbCl_3$ and $CsPbBr_3$ NCs crude solutions, while 2 ml solvent was put in $CsPbI_3$ NCs solution. Then, the solution was centrifuged at 6000 rpm for 5 min. The supernatant was discarded, and the precipitate was centrifuged again at 6000 rpm for 3 min without additional solvent to remove residual supernatant with a paper tissue. Later, the precipitate was redispersed by adding 500 μl of n-hexane and centrifuged again at 4000 rpm for 10min in order to sperate lager particles. The resulting supernatant of $CsPbBr_3$ and $CsPbI_3$ NCs were collected, while the supernatant of $CsPbCl_3$ NCs was discarded. 2 ml n-hexane was loaded into the precipitate to redisperse $CsPbCl_3$ NCs and centrifuged at 4000 rpm for 10 min. Subsequently, the supernatant was collected in a vial. Finally, $CsPbX_3$ (X = Cl, Br, I) NCs were diluted with n-hexane (500 μl, 1ml and 800 μl for $CsPbCl_3$, $CsPbBr_3$ and $CsPbI_3$ NCs, respectively) and filtered by PTFE syringe filters with a 0.45 μm pore size to be uniform.

3.2.4. Anion Exchange Reactions

Shortly, $CsPbBr_3$ was mixed with $CsPbCl_3$ NCs taking different volume ratios. $CsPbBr_3$ was blended with $CsPbI_3$ NCs according to different volume ratios. When the anion exchange was complete, the solutions were transformed into $CsPbBr_xCl_{3-x}$ ($0<x<3$) and $CsPbBr_yI_{3-y}$ ($0<y<3$) NCs, respectively. for 20 min ~ 60 min.

3.3. Materials Characterization

3.3.1. Transmission Electron Microscopy (TEM) Characterization

TEM images were acquired on a JEOL JEM-1400 Plus electron microscope equipped with a thermionic gun at an accelerating voltage of 120 kV. The samples of nanocrystals were prepared by depositing a diluted nanocrystal suspension in n-hexane onto carbon-

 doi:10.20944/preprints202306.0354.v1

coated copper grids. The size distribution images of NCs were calculated by Nano Measurer software.

3.3.2. X-ray Diffraction (XRD) Characterization

XRD analysis was recorded on a Bruker D8 X-ray diffractometer with Cu-Kα radiation (λ = 1.54056 Å, 40 kV and 40 mA). NCs specimens for the XRD measurements were prepared by drop-casting a concentrated NCs suspension in n-hexane onto a SiO_2/Si substrate. XRD data analysis was conducted using the Jade 6.5.

3.3.3. Fourier Transform Infrared (FTIR) Spectroscopy Characterization

Fourier transform infrared (FTIR) spectroscopy were obtained utilizing a Nicolet Model 6700 Fourier transform infrared spectrometer at room temperature. The wave number range of the instrument is chosen to be from 400 to 4000cm^{-1}, the scanning speed is set to 1 time/s, and its maximum resolution is 0.019 cm^{-1}. According to the working principle of interferometer interference frequency modulation, the light emitted from the lamp is turned into interferometric light by Michelson interferometer, and then the interferometric light is allowed to irradiate the sample. The receiver receives the interferometric light with information about materials, which is converted into a Fourier transform by the computer software to obtain a spectral diagram of the sample. For the test, a highly concentrated n-hexane dispersion solution of $CsPbBr_3$ perovskite nanocrystals was applied to the glass slice, which was left to dry and then was tested.

3.3.4. Fluorescence Spectrum Measurements

The UV-vis absorption spectra were carried by a Shimadzu UV-1800 spectrophotometer with UVProbe 2.52 software. The steady-state photoluminescence (PL) spectra were measured on a Shimadzu RF-6000 spectrophotometer with LabSolutions RF software using an excitation wavelength (λ_{ex}) of 350 nm for $CsPbCl_3$, while 450 nm for $CsPbBr_3$ and $CsPbI_3$. Time-resolved photoluminescence spectra (TRPL) were collected by single photon counter. In the procedure of optical characterization, nanocrystals samples were prepared by diluting NCs solutions in n-hexane in quartz cuvettes with a path length of 10 mm.

4. Conclusions

In conclusion, high quality and monodisperse all-inorganic halide perovskite nanocrystals (NCs) with homogeneous cubic morphology and concentrated size distribution, together with a cubic crystal structure, were synthesized by a modified hot injection method with independently modulating the ratio of cesium, lead and halogen precursors. Moreover, we were able to achieve relevant information on the surface functional groups by FTIR spectroscopy, which demonstrated the effective protonation of OAm acting as surface ligands. Different halogen components will contribute to a variation in the band gap of the perovskite NCs and hence varying emission and absorption peak positions in the respective fluorescence spectra and UV-vis absorption spectra. Furthermore, in the fluorescence lifetime curve, the fluorescence lifetime is larger with a red shift of the fluorescence wavelength (band gap) and more slow decay. Nanocrystals mixed from distinct volume ratios undergo anion exchange reactions and consequently exhibit various absorption peaks. In addition, the solution is capable of adjusting in colors from violet to green and from green to red under the stimulation of a UV lamp, covering essentially the entire visible light range. Our work is expected to advance the construction of perovskite materials for optoelectronic devices such as white light-emitting diodes, semiconductor lasers, displays, as well as for serving as photocatalysts for hydrogen generation, CO_2 reduction, and dye degradation.

Supplementary Materials: No supporting information in this article.

Author Contributions: Y.L. conceived projection and material synthetic design. X.W. and J.H. performed the experiment, sample testing, data collection and analysis, X.W. and Y.-Q.L. perform data discussion and formal analyzes, X.W., W.L. and Y. L. wrote, review and edit the manuscript. All authors discussed the results and have agreed to the published version of the manuscript.

Funding: This work is financially supported by National Natural Science Foundation of China (52072281, Y.L.); The Major Program of the National Natural Science Foundation of China (22293021, Y.L.); the National innovation and entrepreneurship training program for college students (No. S202210497011, Y.L.). Y. L. gratefully acknowledges Youth Innovation Research Fund project of State Key Laboratory of Advanced Technology for Materials Synthesis and Processing, Wuhan University of Technology.

Data Availability Statement: Data available in a publicly accessible repository that does not issue DOIs or on request from the corresponding author.

Acknowledgments: We are grateful to the School of Chemical, Chemical and Life Sciences of Wuhan University of Technology for providing UV-Vis and PL characterization, and to the Center for Materials Research and Analysis of Wuhan University of Technology Materials for FTIR testing.

Conflicts of Interest: The authors declare no conflict of interest.

References

1. Akkerman, Q. A.; Manna, L., What Defines a Halide Perovskite? *ACS Energy Lett.* **2020,** *5* (2), 604-610.
2. Zhang, J.; Zhong, Y., Origins of p-Doping and Nonradiative Recombination in $CsSnI_3$. *Angew Chem Int Ed Engl* **2022,** *61* (44), e202212002.
3. Saparov, B.; Mitzi, D. B., Organic-Inorganic Perovskites: Structural Versatility for Functional Materials Design. *Chem Rev* **2016,** *116* (7), 4558-4596.
4. Ceratti, D. R.; Tenne, R.; Bartezzaghi, A.; Cremonesi, L.; Segev, L.; Kalchenko, V.; Oron, D.; Potenza, M. A. C.; Hodes, G.; Cahen, D., Self-Healing and Light-Soaking in MAPbI$_3$: The Effect of H_2O. *Adv Mater* **2022,** *34* (35), e2110239.
5. Li, Y.; Ding, T.; Luo, X.; Tian, Y.; Lu, X.; Wu, K., Synthesis and Spectroscopy of Monodispersed, Quantum-Confined $FAPbBr_3$ Perovskite Nanocrystals. *Chem. Mater.* **2019,** *32* (1), 549-556.
6. Seth, S.; Ahmed, T.; De, A.; Samanta, A., Tackling the Defects, Stability, and Photoluminescence of $CsPbX_3$ Perovskite Nanocrystals. *ACS Energy Lett.* **2019,** *4* (7), 1610-1618.
7. Fu, Y.; Jiang, X.; Li, X.; Traore, B.; Spanopoulos, I.; Katan, C.; Even, J.; Kanatzidis, M. G.; Harel, E., Cation Engineering in Two-Dimensional Ruddlesden-Popper Lead Iodide Perovskites with Mixed Large A-Site Cations in the Cages. *J. Am. Chem. Soc.* **2020,** *142* (8), 4008-4021.
8. Protesescu, L.; Yakunin, S.; Bodnarchuk, M. I.; Krieg, F.; Caputo, R.; Hendon, C. H.; Yang, R. X.; Walsh, A.; Kovalenko, M. V., Nanocrystals of Cesium Lead Halide Perovskites ($CsPbX_3$, X = Cl, Br, and I): Novel Optoelectronic Materials Showing Bright Emission with Wide Color Gamut. *Nano Lett.* **2015,** *15* (6), 3692-3696.
9. Guhrenz, C.; Benad, A.; Ziegler, C.; Haubold, D.; Gaponik, N.; Eychmüller, A., Solid-State Anion Exchange Reactions for Color Tuning of $CsPbX_3$ Perovskite Nanocrystals. *Chem. Mater.* **2016,** *28* (24), 9033-9040.
10. Akkerman, Q. A.; D'Innocenzo, V.; Accornero, S.; Scarpellini, A.; Petrozza, A.; Prato, M.; Manna, L., Tuning the Optical Properties of Cesium Lead Halide Perovskite Nanocrystals by Anion Exchange Reactions. *J. Am. Chem. Soc.* **2015,** *137* (32), 10276-10281.
11. Liu, F.; Zhang, Y.; Ding, C.; Kobayashi, S.; Izuishi, T.; Nakazawa, N.; Toyoda, T.; Ohta, T.; Hayase, S.; Minemoto, T.; Yoshino, K.; Dai, S.; Shen, Q., Highly Luminescent Phase-Stable $CsPbI_3$ Perovskite Quantum Dots Achieving Near 100% Absolute Photoluminescence Quantum Yield. *ACS Nano* **2017,** *11* (10), 10373-10383.
12. Liu, H.; Liu, Z.; Xu, W.; Yang, L.; Liu, Y.; Yao, D.; Zhang, D.; Zhang, H.; Yang, B., Engineering the Photoluminescence of $CsPbX_3$ (X = Cl, Br, and I) Perovskite Nanocrystals Across the Full Visible Spectra with the Interval of 1 nm. *ACS Appl Mater Interfaces* **2019,** *11* (15), 14256-14265.
13. Jiang, Y.; Sun, C.; Xu, J.; Li, S.; Cui, M.; Fu, X.; Liu, Y.; Liu, Y.; Wan, H.; Wei, K.; Zhou, T.; Zhang, W.; Yang, Y.; Yang, J.; Qin, C.; Gao, S.; Pan, J.; Liu, Y.; Hoogland, S.; Sargent, E. H.; Chen, J.; Yuan, M., Synthesis-on-Substrate of Quantum Dot Solids. *Nature* **2022,** *612* (7941), 679-684.
14. Yettapu, G. R.; Talukdar, D.; Sarkar, S.; Swarnkar, A.; Nag, A.; Ghosh, P.; Mandal, P., Terahertz Conductivity within Colloidal $CsPbBr_3$ Perovskite Nanocrystals: Remarkably High Carrier Mobilities and Large Diffusion Lengths. *Nano Lett.* **2016,** *16* (8), 4838-4848.
15. Zhang, X.; Xu, B.; Wang, W.; Liu, S.; Zheng, Y.; Chen, S.; Wang, K.; Sun, X. W., Plasmonic Perovskite Light-Emitting Diodes Based on the Ag-$CsPbBr_3$ System. *ACS Appl Mater Interfaces* **2017,** *9* (5), 4926-4931.
16. Zhang, J.; Zhao, W.; Olthof, S.; Liu, S. F., Defects in $CsPbX_3$ Perovskite: From Understanding to Effective Manipulation for High-Performance Solar Cells. *Small Methods* **2021,** *5* (11), e2100725.

17. Duan, C.; Cui, J.; Zhang, M.; Han, Y.; Yang, S.; Zhao, H.; Bian, H.; Yao, J.; Zhao, K.; Liu, Z.; Liu, S., Precursor Engineering for Ambient-Compatible Antisolvent-Free Fabrication of High-Efficiency $CsPbI_2Br$ Perovskite Solar Cells. *Adv. Energy Mater.* **2020,** *10* (22), 2000691.
18. Zhang, J.; Hodes, G.; Jin, Z.; Liu, S. F., All-Inorganic $CsPbX_3$ Perovskite Solar Cells: Progress and Prospects. *Angew. Chem. Int. Ed.* **2019,** *58* (44), 15596-15618.
19. Ramasamy, P.; Lim, D. H.; Kim, B.; Lee, S. H.; Lee, M. S.; Lee, J. S., All-Inorganic Cesium Lead Halide Perovskite Nanocrystals for Photodetector Applications. *Chem. Commun.* **2016,** *52* (10), 2067-2070.
20. He, Q.; Chen, G.; Wang, Y.; Liu, X.; Xu, D.; Xu, X.; Liu, Y.; Bao, J.; Wang, X., $CsPbX_3$-ITO (X = Cl, Br, I) Nano-Heterojunctions: Voltage Tuned Positive to Negative Photoresponse. *Small* **2021,** *17* (28), e2101403.
21. Li, X.; Wang, Y.; Chen, T.; Xu, T.; Ye, S.; Liu, R.; Sun, Z.; Tan, C.; Lv, X.; Yang, J.; Wang, R.; Ke, S.; Cui, H.; Wen, X.; Wang, C., Unencapsulated $CsPbClBr_2$ Film Photodetectors Grown by Thermal Vacuum Deposition Exhibit Exceptional Environmental Stability in High-Humidity Air. *ACS Appl Energy Mater* **2022,** *5* (7), 8709-8716.
22. Wang, Z.; Yang, J.; Li, M.; Zeng, X.; Pi, M.; Liu, Z.; Liu, J.; Zhang, D.; Hu, Z.; Du, J., Low Threshold and Ultrastability of One-Step Air-Processed All-Inorganic $CsPbX_3$ Thin Films toward Full-Color Visible Amplified Spontaneous Emission. *ACS Appl Mater Interfaces* **2022,** *14* (23), 26904-26912.
23. Nie, L.; Yu, X.; Ge, Y.; He, D.; Zhu, X.; Liu, H.; Guo, H.; Zhao, F.; Yu, S.; Qiu, J.; Xu, X.; Wang, T., Highly Stable and Controllable Lasing Actions from PVDF Encapsulated $CsPbBr_3$ Perovskite Microcrystals. *J. Mater. Chem. C* **2022,** *10* (43), 16301-16308.
24. Wang, Y.; Li, X.; Nalla, V.; Zeng, H.; Sun, H., Solution-Processed Low Threshold Vertical Cavity Surface Emitting Lasers from All-Inorganic Perovskite Nanocrystals. *Adv. Funct. Mater.* **2017,** *27* (13), 1605088.
25. Yang, X.; Zhang, X.; Deng, J.; Chu, Z.; Jiang, Q.; Meng, J.; Wang, P.; Zhang, L.; Yin, Z.; You, J., Efficient Green Light-Emitting Diodes Based on Quasi-Two-Dimensional Composition and Phase Engineered Perovskite with Surface Passivation. *Nat Commun* **2018,** *9* (1), 570.
26. Cao, Y.; Wang, N.; Tian, H.; Guo, J.; Wei, Y.; Chen, H.; Miao, Y.; Zou, W.; Pan, K.; He, Y.; Cao, H.; Ke, Y.; Xu, M.; Wang, Y.; Yang, M.; Du, K.; Fu, Z.; Kong, D.; Dai, D.; Jin, Y.; Li, G.; Li, H.; Peng, Q.; Wang, J.; Huang, W., Perovskite Light-Emitting Diodes Based on Spontaneously Formed Submicrometre-Scale Structures. *Nature* **2018,** *562* (7726), 249-253.
27. Lin, K.; Xing, J.; Quan, L. N.; de Arquer, F. P. G.; Gong, X.; Lu, J.; Xie, L.; Zhao, W.; Zhang, D.; Yan, C.; Li, W.; Liu, X.; Lu, Y.; Kirman, J.; Sargent, E. H.; Xiong, Q.; Wei, Z., Perovskite Light-emitting Diodes with External Quantum Efficiency Exceeding 20 Percent. *Nature* **2018,** *562* (7726), 245-248.
28. Wang, K.; Zhang, H.; Gu, Z., All-Inorganic Perovskite Nanocrystal Materials: New Generation of Scintillators for High Quality X-ray Imaging. *Sci Bull* **2019,** *64* (17), 1205-1206.
29. Ma, W.; Jiang, T.; Yang, Z.; Zhang, H.; Su, Y.; Chen, Z.; Chen, X.; Ma, Y.; Zhu, W.; Yu, X.; Zhu, H.; Qiu, J.; Liu, X.; Xu, X.; Yang, Y. M., Highly Resolved and Robust Dynamic X-Ray Imaging Using Perovskite Glass-Ceramic Scintillator with Reduced Light Scattering. *Adv Sci* **2021,** *8* (15), e2003728.
30. Yang, H.; Li, H.; Yuan, R.; Chen, J.; Zhao, J.; Wang, S.; Liu, Y.; Li, Q.; Zhang, Z., A Novel Scintillation Screen for Achieving High-Energy Ray Detection with Fast and Full-Color Emission. *J. Mater. Chem. C* **2021,** *9* (25), 7905-7909.
31. Chan, K. K.; Giovanni, D.; He, H.; Sum, T. C.; Yong, K.-T., Water-Stable All-Inorganic Perovskite Nanocrystals with Nonlinear Optical Properties for Targeted Multiphoton Bioimaging. *ACS Appl Nano Mater* **2021,** *4* (9), 9022-9033.
32. Kar, M. R.; Kumar, S.; Acharya, T. K.; Goswami, C.; Bhaumik, S., Highly Water-Stable, Luminescent, and Monodisperse Polymer-Coated $CsPbBr_3$ Nanocrystals for Imaging in Living Cells with Better Sensitivity. *RSC Adv* **2023,** *13* (9), 5946-5956.
33. Mohapatra, A.; Kumar, S.; Acharya, T. K.; Goswami, C.; Bhaumik, S., Highly Stable Multi-Encapsulated Red-Emitting Cesium Lead Halide Nanocrystals for Efficient Copper Ion Detection and Imaging in Live Cells. *J. Alloys Compd.* **2023,** *947*, 169453.
34. Xiao, M.; Hao, M.; Lyu, M.; Moore, E. G.; Zhang, C.; Luo, B.; Hou, J.; Lipton‐Duffin, J.; Wang, L., Surface Ligands Stabilized Lead Halide Perovskite Quantum Dot Photocatalyst for Visible Light‐Driven Hydrogen Generation. *Adv. Funct. Mater.* **2019,** *29* (48).
35. Yang, Y.; Li, Y.; Gong, W.; Guo, H.; Niu, X., Cobalt-doped CsPbBr3 perovskite quantum dots for photoelectrocatalytic hydrogen production via efficient charge transport. *Colloids Surf., A* **2023,** *663*.
36. Pavliuk, M. V.; Abdellah, M.; Sá, J., Hydrogen Evolution with $CsPbBr_3$ Perovskite Nanocrystals under Visible Light in Solution. *Mater Today Commun* **2018,** *16*, 90-96.
37. Xu, Y. F.; Yang, M. Z.; Chen, B. X.; Wang, X. D.; Chen, H. Y.; Kuang, D. B.; Su, C. Y., A $CsPbBr_3$ Perovskite Quantum Dot/Graphene Oxide Composite for Photocatalytic CO_2 Reduction. *J Am Chem Soc* **2017,** *139* (16), 5660-5663.
38. Hou, J.; Cao, S.; Wu, Y.; Gao, Z.; Liang, F.; Sun, Y.; Lin, Z.; Sun, L., Inorganic Colloidal Perovskite Quantum Dots for Robust Solar CO_2 Reduction. *Chem* **2017,** *23* (40), 9481-9485.
39. Li, L.; Zhang, Z.; Ding, C.; Xu, J., Boosting charge separation and photocatalytic CO_2 reduction of $CsPbBr_3$ perovskite quantum dots by hybridizing with P3HT. *Chem. Eng. J.* **2021,** *419*.
40. Liu, H.; Bansal, S., Metal halide perovskite nanostructures and quantum dots for photocatalytic CO_2 reduction: prospects and challenges. *Mater. Today Energy* **2023,** *32*.
41. Das, S.; Paul, T.; Maiti, S.; Chattopadhyay, K. K., Ambient Processed $CsPbX_3$ Perovskite Cubes for Photocatalysis. *Mater. Lett.* **2020,** *267*, 127501.
42. Gao, G.; Xi, Q.; Zhou, H.; Zhao, Y.; Wu, C.; Wang, L.; Guo, P.; Xu, J., Novel inorganic perovskite quantum dots for photocatalysis. *Nanoscale* **2017,** *9* (33), 12032-12038.

43. Xin, B.; Pak, Y.; Mitra, S.; Almalawi, D.; Alwadai, N.; Zhang, Y.; Roqan, I. S., Self-Patterned $CsPbBr_3$ Nanocrystals for High-Performance Optoelectronics. *ACS Appl Mater Interfaces* **2019,** *11* (5), 5223-5231.
44. Fu, X.; Zhang, C.; Peng, Z.; Xia, Y.; Zhang, J.; Luo, W.; Zhan, R.; Li, H.; Wang, Y.; Zhang, D., Self-Assembly and Photoactivation of Blue Luminescent $CsPbBr_3$ Mesocrystals Synthesized at Ambient Temperature. *J. Mater. Chem. C* **2018,** *6* (7), 1701-1708.
45. Liu, X.; Li, J.; Cui, X.; Wang, X.; Yang, D., Strategies for the Preparation of High-Performance Inorganic Mixed-Halide Perovskite Solar Cells. *RSC Adv* **2022,** *12* (51), 32925-32948.
46. Wang, Y.; Yasar, M.; Luo, Z.; Zhou, S.; Yu, Y.; Li, H.; Yang, R.; Wang, X.; Pan, A.; Gan, L.; Zhai, T., Temperature Difference Triggering Controlled Growth of All-Inorganic Perovskite Nanowire Arrays in Air. *Small* **2018,** *14* (41), e1803010.
47. Dong, S.; Hu, Z. Y.; Wei, P.; Han, J.; Wang, Z.; Liu, J.; Su, B. L.; Zhao, D.; Liu, Y., All-Inorganic Perovskite Single-Crystal Photoelectric Anisotropy. *Adv Mater* **2022,** *34* (37), e2204342.
48. Sun, S.; Yuan, D.; Xu, Y.; Wang, A.; Deng, Z., Ligand-Mediated Synthesis of Shape-Controlled Cesium Lead Halide Perovskite Nanocrystals via Reprecipitation Process at Room Temperature. *ACS Nano* **2016,** *10* (3), 3648-3657.
49. Pan, A.; He, B.; Fan, X.; Liu, Z.; Urban, J. J.; Alivisatos, A. P.; He, L.; Liu, Y., Insight into the Ligand-Mediated Synthesis of Colloidal $CsPbBr_3$ Perovskite Nanocrystals: The Role of Organic Acid, Base, and Cesium Precursors. *ACS Nano* **2016,** *10* (8), 7943-7954.
50. Chen, D.; Fang, G.; Chen, X.; Lei, L.; Zhong, J.; Mao, Q.; Zhou, S.; Li, J., Mn-Doped $CsPbCl_3$ Perovskite Nanocrystals: Solvothermal Synthesis, Dual-Color Luminescence and Improved Stability. *J. Mater. Chem. C* **2018,** *6* (33), 8990-8998.
51. Chen, M.; Zou, Y.; Wu, L.; Pan, Q.; Yang, D.; Hu, H.; Tan, Y.; Zhong, Q.; Xu, Y.; Liu, H.; Sun, B.; Zhang, Q., Solvothermal Synthesis of High-Quality All-Inorganic Cesium Lead Halide Perovskite Nanocrystals: From Nanocube to Ultrathin Nanowire. *Adv. Funct. Mater.* **2017,** *27* (23), 1701121.
52. Han, D.; Imran, M.; Zhang, M.; Chang, S.; Wu, X. G.; Zhang, X.; Tang, J.; Wang, M.; Ali, S.; Li, X.; Yu, G.; Han, J.; Wang, L.; Zou, B.; Zhong, H., Efficient Light-Emitting Diodes Based on in Situ Fabricated $FAPbBr_3$ Nanocrystals: The Enhancing Role of the Ligand-Assisted Reprecipitation Process. *ACS Nano* **2018,** *12* (8), 8808-8816.
53. Dang, Z.; Shamsi, J.; Akkerman, Q. A.; Imran, M.; Bertoni, G.; Brescia, R.; Manna, L., Low-Temperature Electron Beam-Induced Transformations of Cesium Lead Halide Perovskite Nanocrystals. *ACS Omega* **2017,** *2* (9), 5660-5665.
54. Li, F.; Liu, Y.; Wang, H.; Zhan, Q.; Liu, Q.; Xia, Z., Postsynthetic Surface Trap Removal of $CsPbX_3$ (X = Cl, Br, or I) Quantum Dots via a ZnX_2/Hexane Solution toward an Enhanced Luminescence Quantum Yield. *Chem. Mater.* **2018,** *30* (23), 8546-8554.
55. Yu, Y.; Zhang, D.; Kisielowski, C.; Dou, L.; Kornienko, N.; Bekenstein, Y.; Wong, A. B.; Alivisatos, A. P.; Yang, P., Atomic Resolution Imaging of Halide Perovskites. *Nano Lett.* **2016,** *16* (12), 7530-7535.
56. Chen, Y.-C.; Chou, H.-L.; Lin, J.-C.; Lee, Y.-C.; Pao, C.-W.; Chen, J.-L.; Chang, C.-C.; Chi, R.-Y.; Kuo, T.-R.; Lu, C.-W.; Wang, D.-Y., Enhanced Luminescence and Stability of Cesium Lead Halide Perovskite $CsPbX_3$ Nanocrystals by Cu^{2+}-Assisted Anion Exchange Reactions. *J Phy Chem C* **2019,** *123* (4), 2353-2360.
57. Uddin, M. A.; Glover, J. D.; Park, S. M.; Pham, J. T.; Graham, K. R., Growth of Highly Stable and Luminescent $CsPbX_3$ (X = Cl, Br, and I) Nanoplates via Ligand Mediated Anion Exchange of $CsPbCl_3$ Nanocubes with AlX_3. *Chem. Mater.* **2020,** *32* (12), 5217-5225.
58. Imran, M.; Caligiuri, V.; Wang, M.; Goldoni, L.; Prato, M.; Krahne, R.; De Trizio, L.; Manna, L., Benzoyl Halides as Alternative Precursors for the Colloidal Synthesis of Lead-Based Halide Perovskite Nanocrystals. *J. Am. Chem. Soc.* **2018,** *140* (7), 2656-2664.